Photoswitchable diacylglycerols enable optical control of protein translocation, PKC activity, and vesicle release

James Allen Frank[1], Dmytro A. Yushchenko[2,3], David J. Hodson[4,5,6], Noa Lipstein[7], Jatin Nagpal[8,9], Guy A. Rutter[4], Jeong-Seop Rhee[7], Alexander Gottschalk[8,9], Nils Brose[7], Carsten Schultz*[2], Dirk Trauner*[1]

[1]Department of Chemistry and Center for Integrated Protein Science, Ludwig Maximilians University Munich, Butenandtstraße 5-13, 81377 Munich, Germany. [2]European Molecular Biology Laboratory (EMBL), Cell Biology & Biophysics Unit, Meyerhofstraße 1, 69117 Heidelberg, Germany. [3]Institute of Organic Chemistry and Biochemistry, Academy of Sciences of the Czech Republic, Flemingovo namesti 2, 16610 Prague 6, Czech Republic. [4]Section of Cell Biology and Functional Genomics, Department of Medicine, Imperial College London, ICTEM, Hammersmith Hospital, Du Cane Road, London W12 0NN, UK. [5]Institute of Metabolism and Systems Research (IMSR), University of Birmingham, Birmingham B15 2TT, UK. [6]Centre for Endocrinology, Diabetes and Metabolism, Birmingham Health Partners, Birmingham, B15 2TH, England. [7]Department of Molecular Neurobiology, Max Planck Institute of Experimental Medicine, Hermann-Rein Straße 3, 37075 Göttingen, Germany. [8]Buchmann Institute for Molecular Life Sciences, Goethe University, Max von Laue Strasse 15, D-60438 Frankfurt, Germany. [9]Institute of Biochemistry, Department for Biochemistry, Chemistry and Pharmacy, Goethe University, Max von Laue Strasse 9, D-60438 Frankfurt, Germany.

SUPPORTING INFORMATION

SUPPLEMENTARY FIGURES

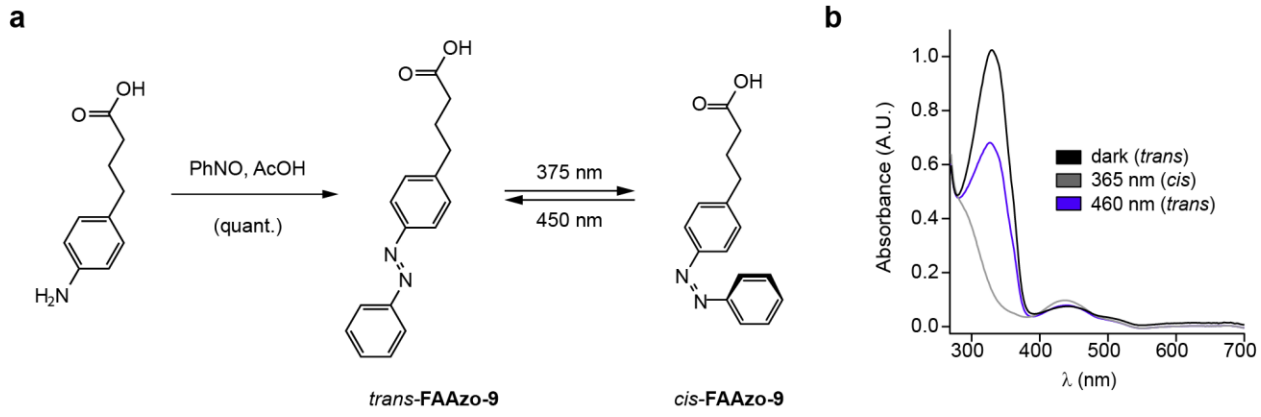

Supplementary Figure 1 | Synthesis and characterization of a short-chain photoswitchable fatty acid. (**a**) The chemical synthesis of **FAAzo-9**. (**b**) UV-Vis spectroscopy showed that **FAAzo-9** (50 μM in DMSO) could be isomerized between its *cis*- and *trans*-configurations with UV-A and blue light, respectively. Absorption spectra are shown for the *dark*-adapted (black), *UV*-adapted (grey) and *blue*-adapted (blue) photostationary states.

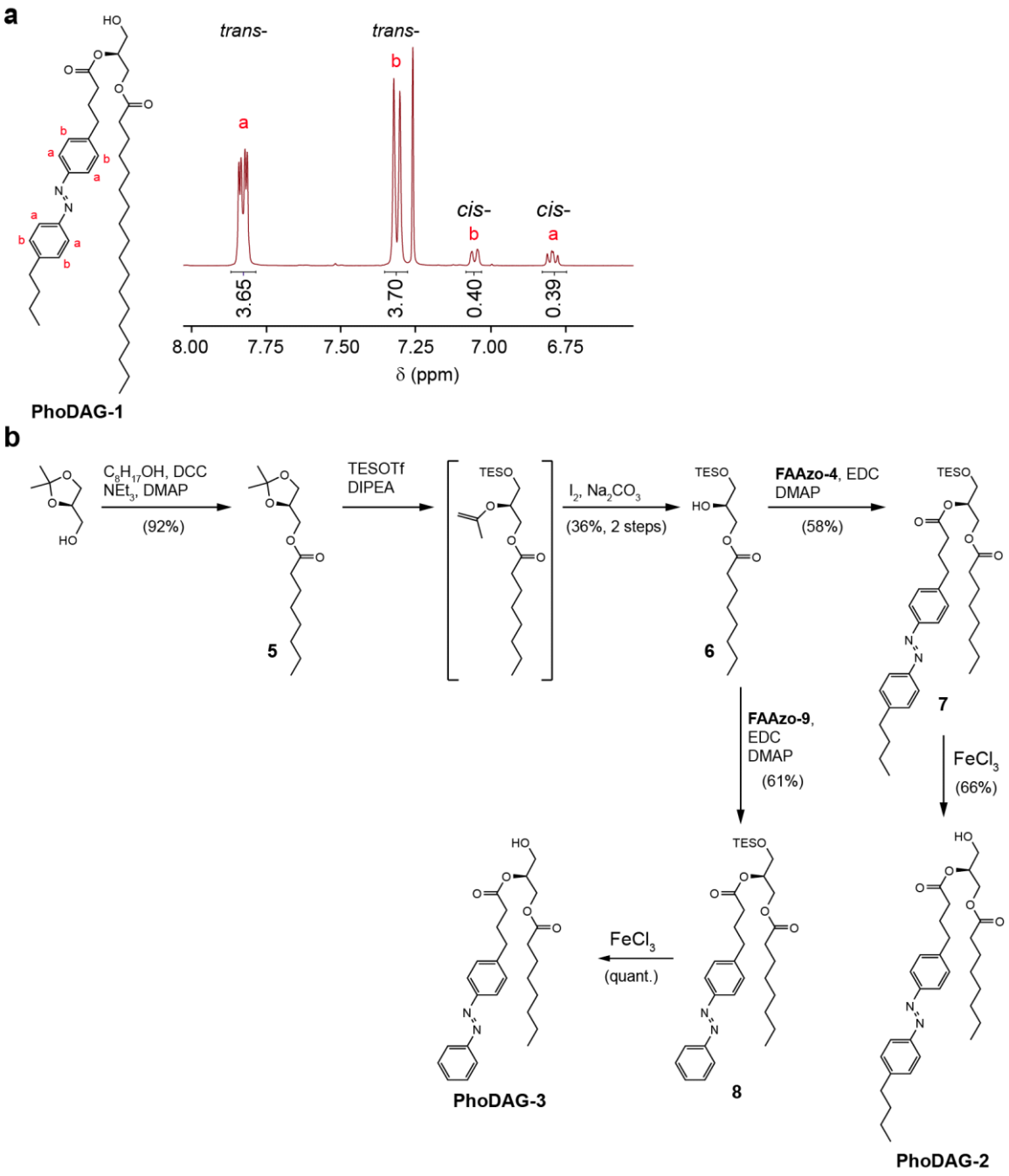

Supplementary Figure 2 | Synthesis and characterization of the photoswitchable diacylglycerols. (**a**) A representative NMR spectrum of **PhoDAG-1** (in $CDCl_3$), displaying the aromatic region. Both the *trans*- and *cis*- azobenzene protons give signals under ambient lighting conditions, where **PhoDAG-1** exists as ≈10% the *cis*-isomer. (**b**) The chemical syntheses of the short-chain photoswitchable DAGs, **PhoDAG-2** and **PhoDAG-3**.

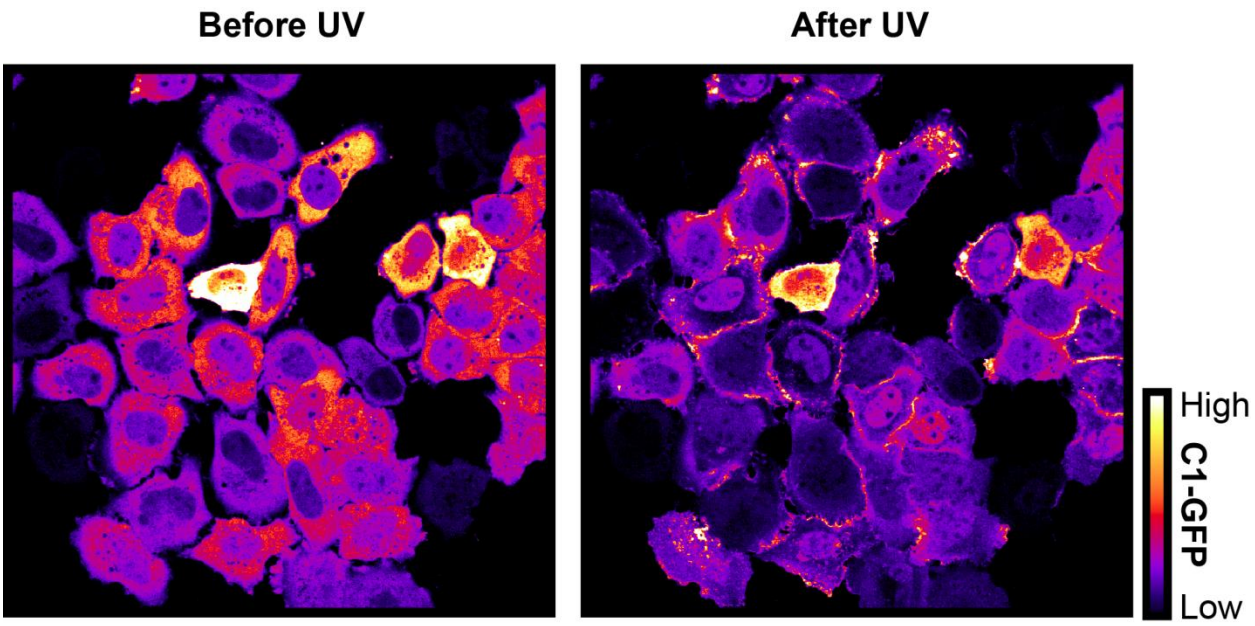

Supplementary Figure 3 | Optical control of C1-GFP translocation. In HeLa cells expressing C1-GFP, **PhoDAG-1** (150 μM) triggered the translocation of C1-GFP towards the plasma membrane on irradiation with λ = 375 nm laser light.

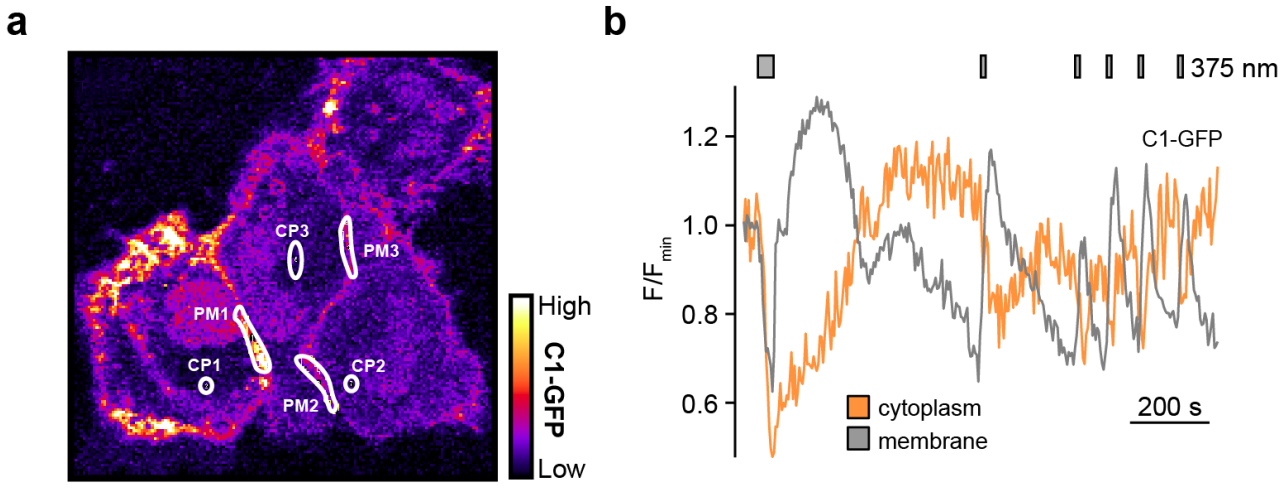

Supplementary Figure 4 | Quantification of C1-GFP translocation. (**a**) A representative fluorescence image detailing the cytoplasmic (CP) and plasma membrane (PM) sample regions used for translocation quantification. Displayed here is C1-GFP fluorescence after the application of **PhoDAG-1** (400 μM) and λ = 375 nm irradiation. (**b**) The GFP fluorescence intensities at the plasma membrane and cytoplasm of a representative cell after the application of **PhoDAG-1** (200 μM).

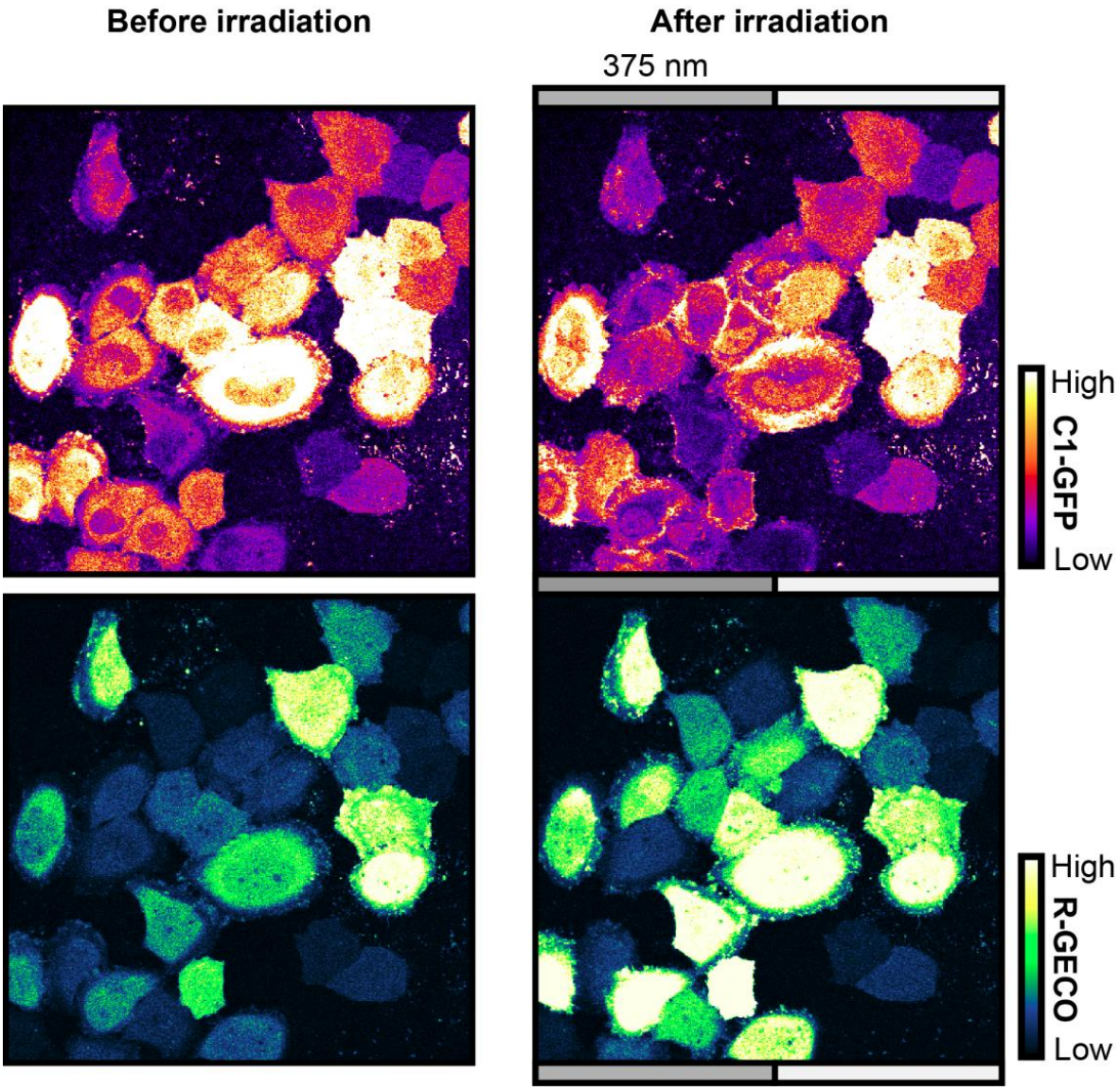

Supplementary Figure 5 | PhoDAG-1 enables spatial control of DAG signaling. In HeLa cells expressing C1-GFP and R-GECO, **PhoDAG-1** (150 μM) activation could be targeted to specific cells. In this case, only the left half of the field of view (gray bar) was photoactivated with λ = 375 nm irradiation. In these cells, C1-GFP translocated towards the plasma membrane, alongside an increase in intracellular Ca^{2+} levels. The right half of the frame remained largely unaffected (white bar).

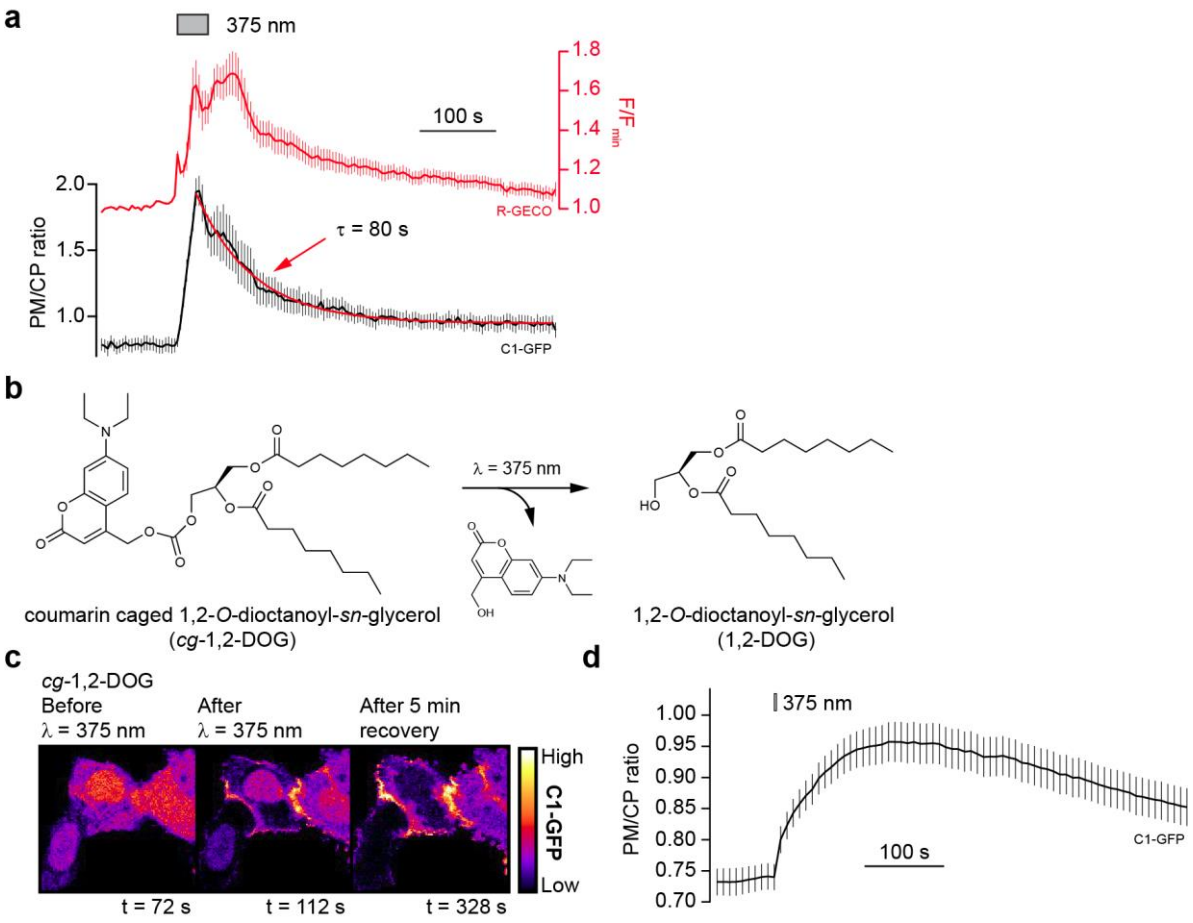

Supplementary Figure 6 | Optical control of C1-GFP translocation in HeLa cells. (**a**) HeLa cells expressing C1-GFP and R-GECO were incubated **PhoDAG-1** (150 μM) followed by washing with buffer to remove extracellular compound. Translocation of C1-GFP towards the plasma membrane was observed on irradiation with λ = 375 nm light. An increase in intracellular Ca^{2+} was also observed in the same cells (n = 12). (**b**) The chemical structure of 1,2-*O*-dioctanoyl-*sn*-glycerol (1,2-DOG) being liberated from caged 1,2-DOG (*cg*-1,2-DOG) on irradiation with λ = 375 nm laser light. (**c**,**d**) The uncaging of *cg*-1,2-DOG (100 μM) led to C1-GFP translocation towards the plasma membrane in HeLa cells. After uncaging, the recovery was relatively slow. Shown are (**c**) fluorescence images of two representative cells, and (**d**) data averaged from multiple cells (n = 25), displayed as the plasma membrane to cytoplasm (PM/CP) fluorescence ratio. Error bars were calculated as s.e.m.

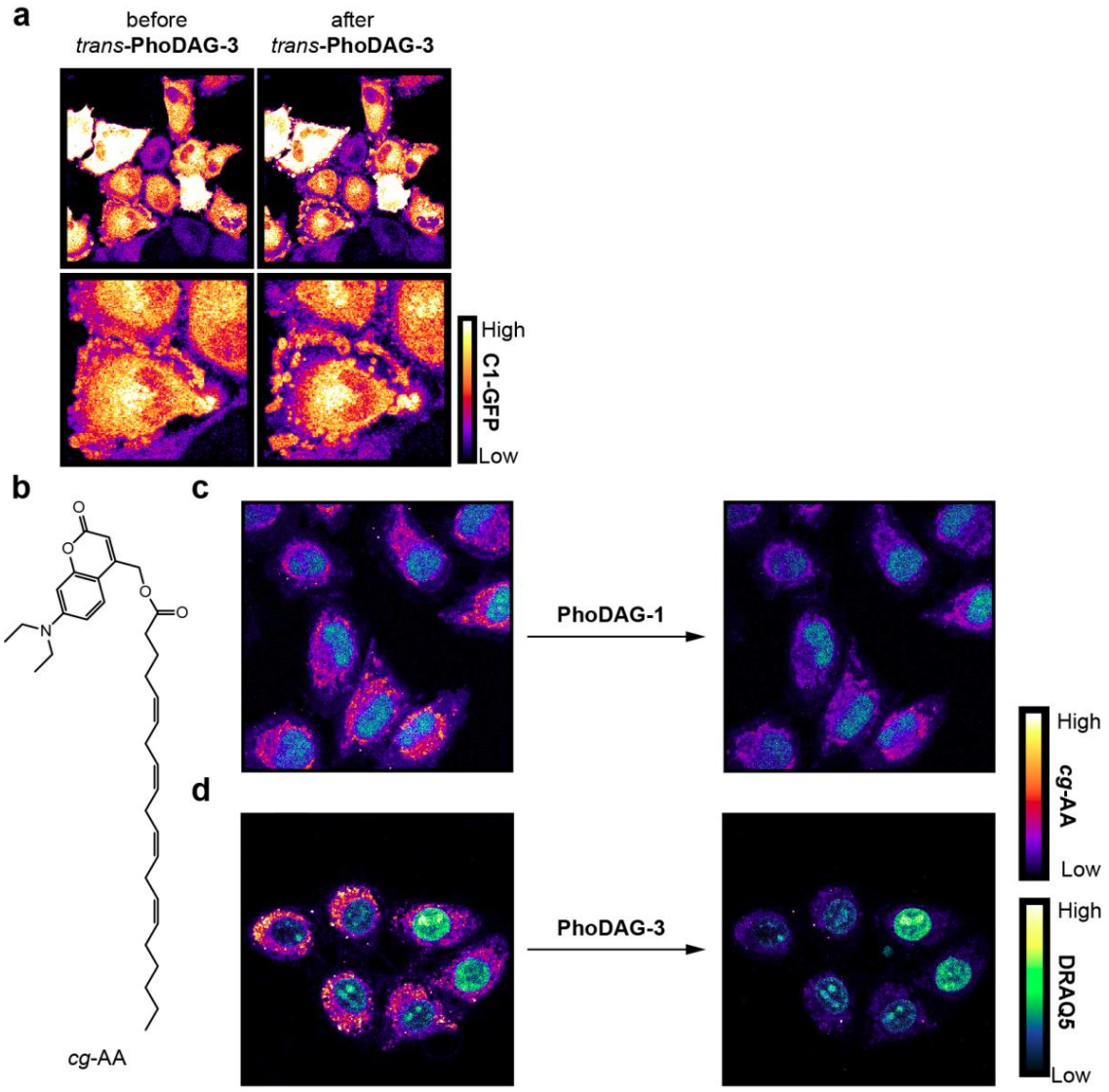

Supplementary Figure 7 | Lipid chain length determines the localization and activity of the PhoDAGs. (**a**) In HeLa cells, *trans*-**PhoDAG-3** (150 μM) caused translocation of C1-GFP towards internal membranes on application. (**b**) The chemical structure of coumarin-labeled arachidonic acid (*cg*-AA), which localizes in internal membranes. (**c**,**d**) Representative fluorescence images showing the localization of *cg*-AA (100 μM, fire) before (left) and after (right) the addition of (**c**) **PhoDAG-1** (150 μM) or (**d**) **PhoDAG-3** (150 μM). **PhoDAG-3** quenched the coumarin fluorescence significantly more quickly than **PhoDAG-1**. Cell nuclei were stained with DRAQ-5 (green) as a reference.

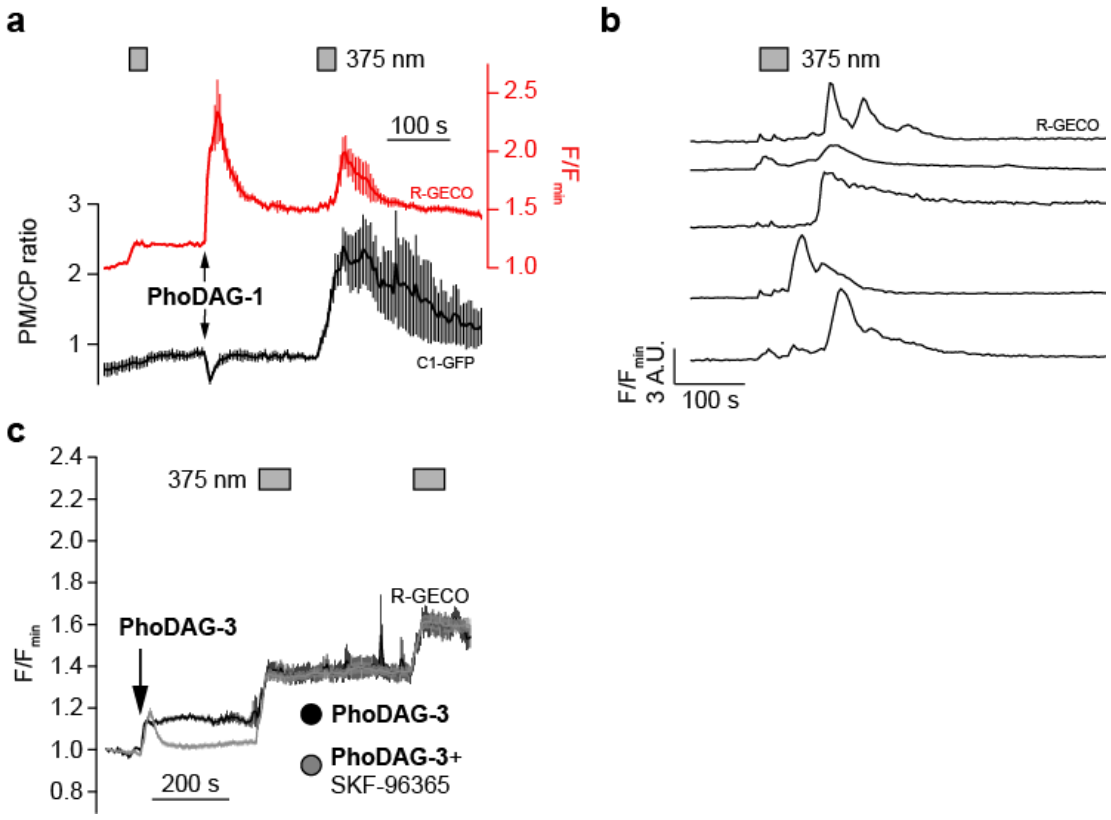

Supplementary Figure 8 | PhoDAG-1 induces an increase in intracellular Ca^{2+} in HeLa cells. HeLa cells were transfected with C1-GFP and R-GECO. (**a**) Before the application of **PhoDAG-1**, UV-A irradiation alone did not catalyze C1-GFP translocation. Application of *trans*-**PhoDAG-1** (300 μM) caused an increase in intracellular Ca^{2+} ($[Ca^{2+}]_i$) levels, however no translocation was observed until triggered by λ = 375 nm irradiation (n = 6). (**b**) On photoactivation, a small increase in $[Ca^{2+}]_i$ was observed, followed by a delayed, larger Ca^{2+} increase, displayed as representative traces from individual cells. (**c**) The TRPC channel inhibitor SKF-96365 (50 μM) slightly decreased the Ca^{2+} influx after application of **PhoDAG-3** (150 μM), but not on photoactivation (n = 54, gray), when compared to **PhoDAG-3** alone (n = 16, black). Translocation is represented as the plasma membrane to cytoplasm (PM/CP) C1-GFP fluorescence ratio, while Ca^{2+} levels were plotted as the R-GECO fluorescence intensity normalized to the baseline fluorescence (F/F_{min}). Error bars were calculated as s.e.m.

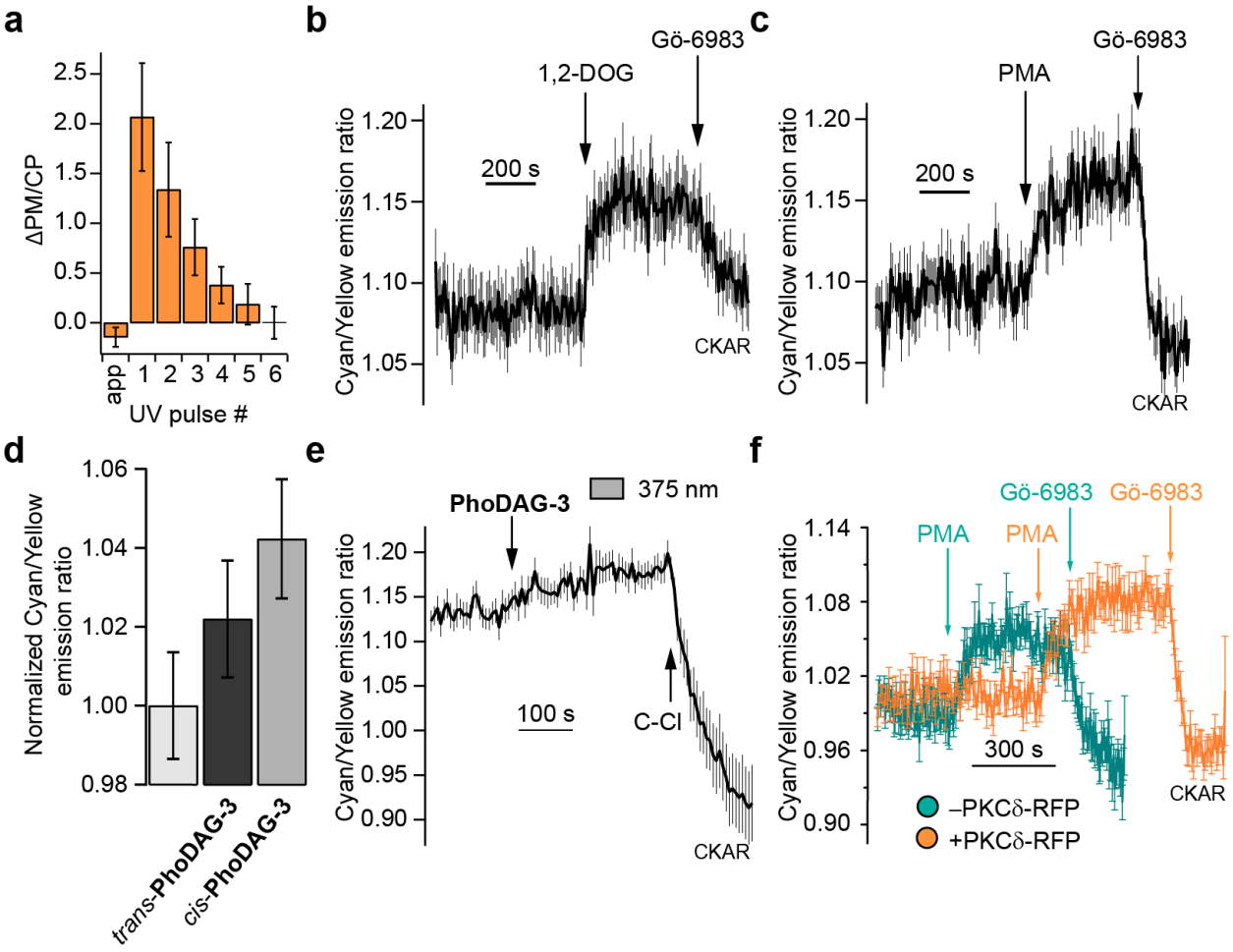

Supplementary Figure 9 | Optical control of protein kinase C. (**a**) In HeLa cells expressing PKCδ-RFP, translocation efficiency induced by **PhoDAG-1** (100 μM) decayed over multiple cycles of irradiation of the same length (28 s pulses at λ = 375 nm, n = 11). (**b**,**c**) As shown by the cytosolic C Kinase Activity Reporter (CKAR), the application of (**b**) 1,2-DOG (300 μM, n = 32) and (**c**) phorbol 12-myristate 13-acetate (PMA, 5 μM, n = 31) produced an increase in the CFP/YFP emission ratio, indicating kinase activation. In both cases, the FRET change was immediately reversed on addition of the broadband PKC inhibitor Gö-6983 (10 μM). (**d**,**e**) **PhoDAG-3** (15 μM) caused an increase in the CFP/YFP emission ratio on application, and a further increase on photoactivation. This effect was reversed by the application of chelerythrine chloride (C-Cl, 100 μM) (n = 14). (**f**) The CKAR response in HeLa cells was compared between cells with (n = 37 orange) and without (n = 20, teal) the expression of exogenous PKCδ-RFP. Overexpression of PKCδ-RFP increased the CKAR response by 1.2 fold when compared to endogenous PKC expression only. Error bars were calculated as s.e.m.

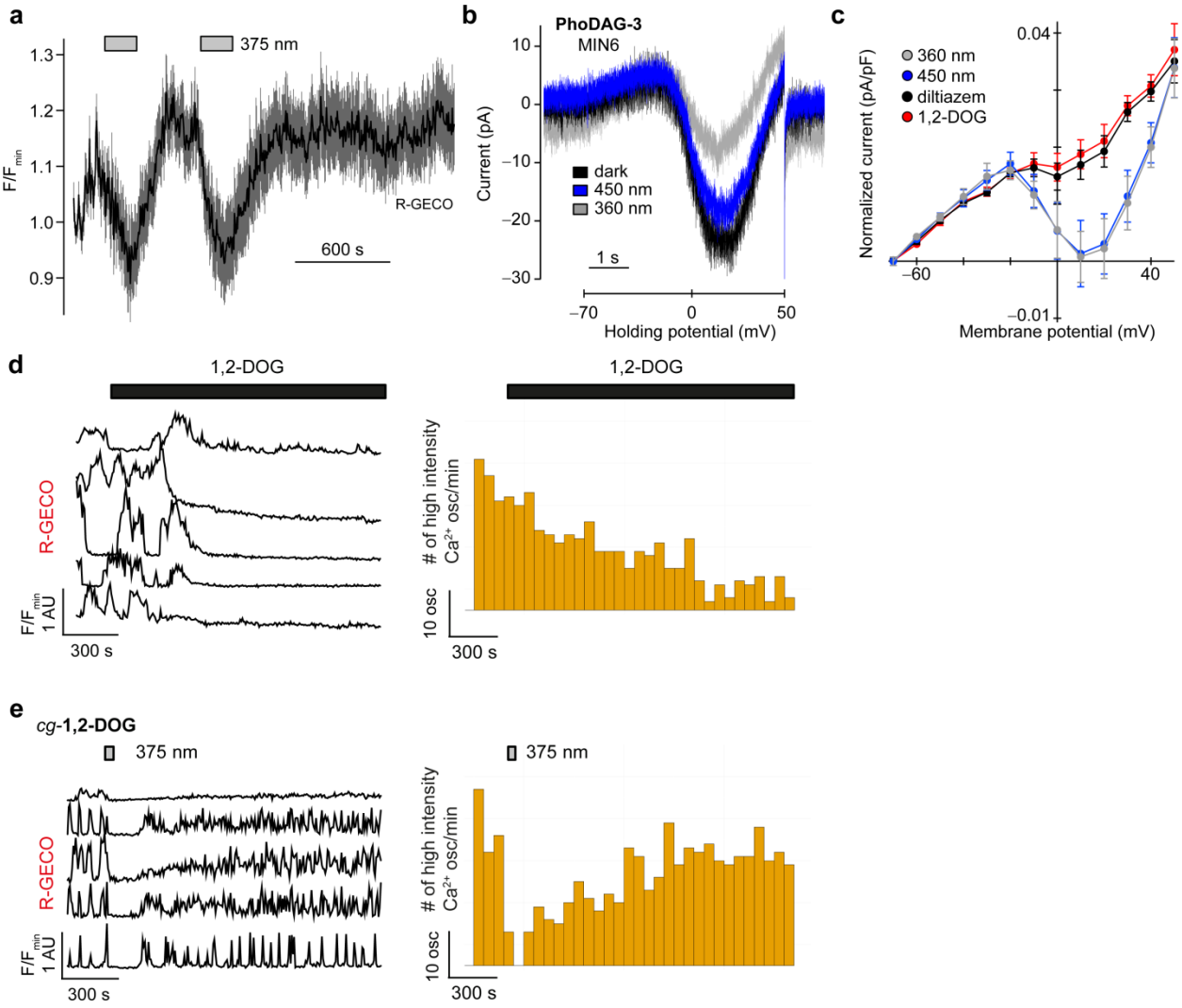

Supplementary Figure 10 | Diacylglycerol generation decreases Ca^{2+} oscillations in MIN6 cells. Ca^{2+} oscillations in glucose stimulated (20 mM) MIN6 cells were monitored using R-GECO (**a**) **PhoDAG-1** (300 μM) caused a decrease in the overall $[Ca^{2+}]_i$ level on photoactivation. Data was averaged over multiple cells (n = 23). (**b**) **PhoDAG-3** (35 μM) triggered a decrease in the whole-cell voltage activated L-type Ca^{2+} channel (Ca_v) current, as shown by voltage ramps (–70 to +50 mV over 5 s) from a representative cell. (**c**) UV-A or blue irradiation alone did not affect the Ca_v current (n = 8), while the application of 1,2-DOG (100 μM, n = 3) and the L-type Ca^{2+} channel blocker diltiazem (500 μM, n = 3) decreased the magnitude of the whole-cell Ca_v current. (**d**) The application of 1,2-*O*-dioctanoyl-*sn*-glycerol (1,2-DOG, 100 μM) led to a slow and permanent decrease in the frequency and intensity of Ca^{2+} oscillations (n = 25). (**e**) After the uncaging of caged 1,2-DOG (*cg*-1,2-DOG, 100 μM), the frequency and intensity of the Ca^{2+} oscillations was immediately reduced, but recovered gradually over 20-30 min (n = 47). Bar graphs represent the number of detected high intensity Ca^{2+} oscillations (>50% of highest transient in each trace) within every 60 s interval. Error bars were calculated as s.e.m.

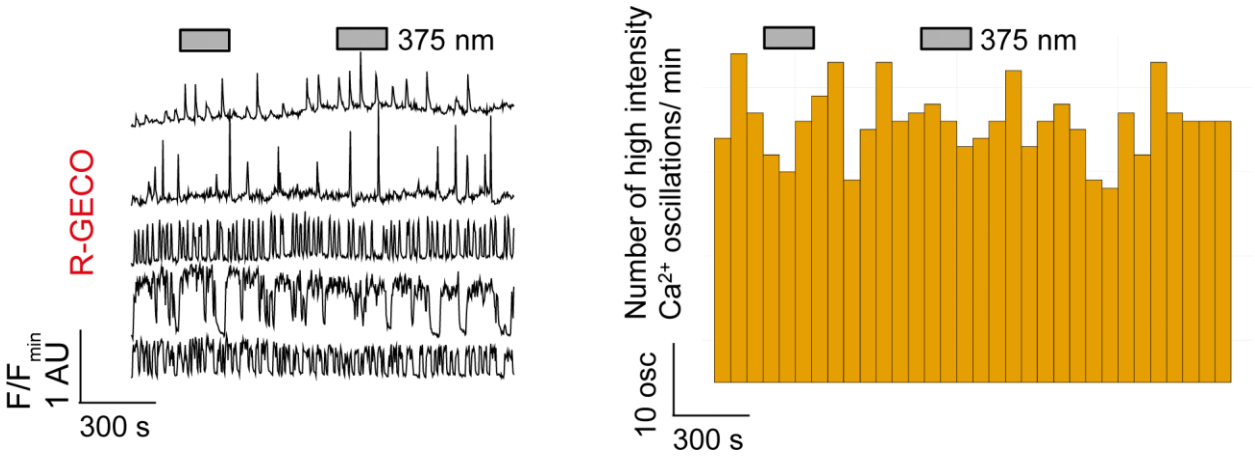

Supplementary Figure 11 | UV-A illumination of MIN6 cells alone has no significant effect on Ca^{2+} oscillations. Ca^{2+} oscillations in glucose-stimulated (20 mM) MIN6 cells were monitored using R-GECO. Shown are individual Ca^{2+} traces from representative cells (left), and a statistical analysis of the oscillation frequency averaged over multiple cells (right). Bar graphs represent the number of detected high intensity Ca^{2+} oscillations (>50% of highest transient in each trace) within every 60 s interval.

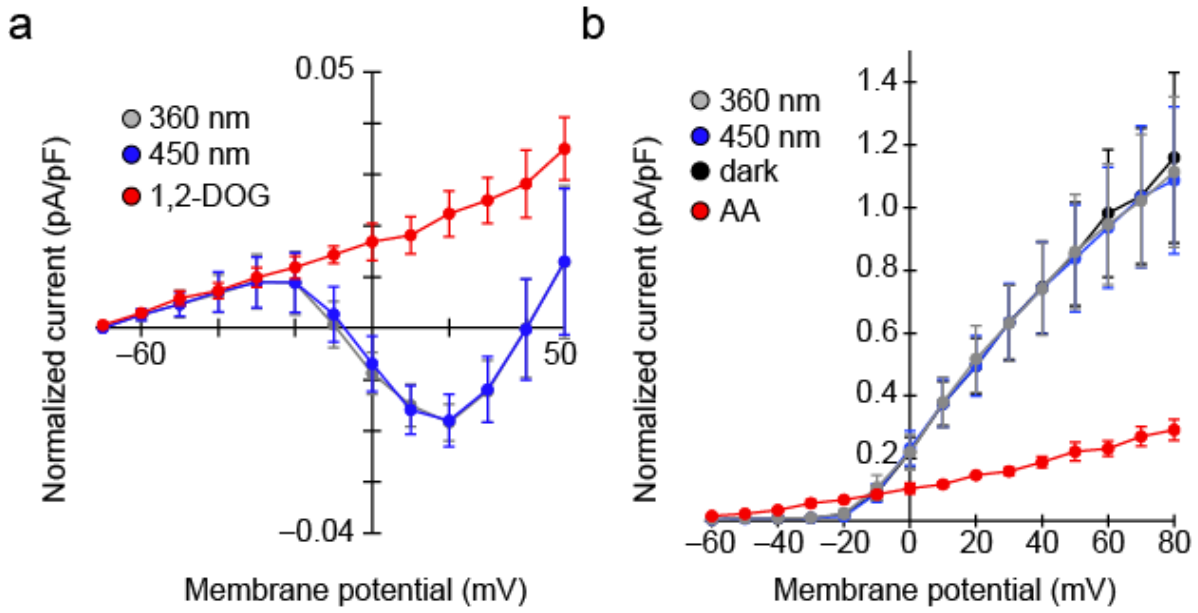

Supplementary Figure 12 | Control experiments for electrophysiological studies in dissociated β-cells. In primary mouse β-cells: (**a**) UV-A or blue-irradiation did not affect the Ca_v current (n = 8), while the application of 1,2-DOG (15 μM) decreased the magnitude of the Ca_v current (n = 3). (**b**) UV-A or blue-irradiation also did not affect the delayed rectifier voltage-gated K^+ channel (K_v) current (n = 4). Arachidonic acid (AA, 10 μM) decreased the magnitude of the K_v current (n = 4). Error bars were calculated as s.e.m.

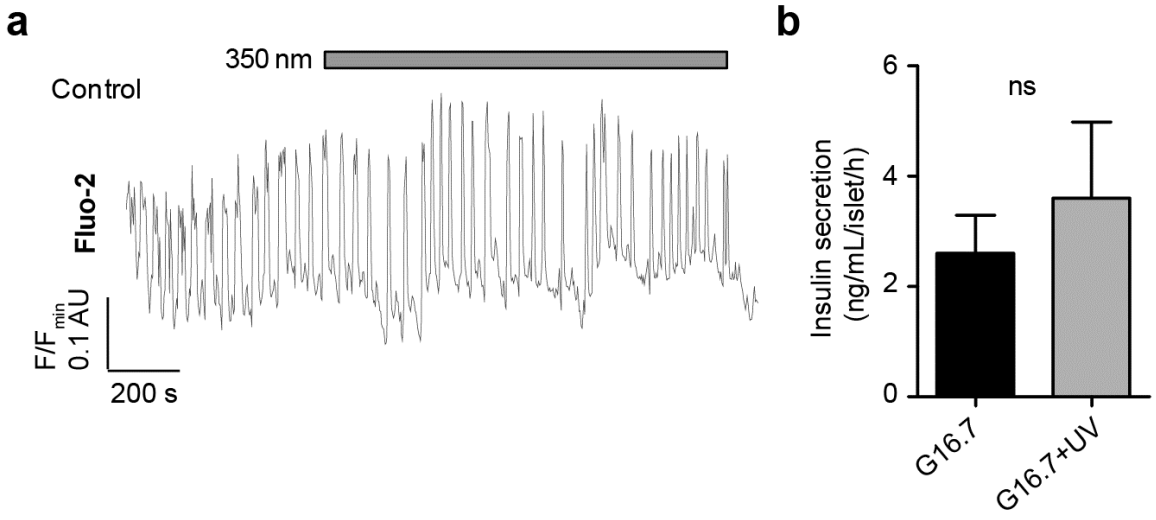

Supplementary Figure 13 | UV-A irradiation alone does not alter glucose-stimulated pancreatic islet activity. Ca^{2+} oscillations in intact mouse pancreatic islets were monitored by Fluo-2. UV-A irradiation (λ = 350 nm) alone did not affect (**a**) the speed of the Ca^{2+} oscillations in islets stimulated by 11 mM glucose or (**b**) the insulin secretion stimulated by 16.7 mM glucose (G16.7) (n = 3 experiments from 3 animals). ns = not significant P>0.05, P>0.05. Error bars were calculated as s.e.m.

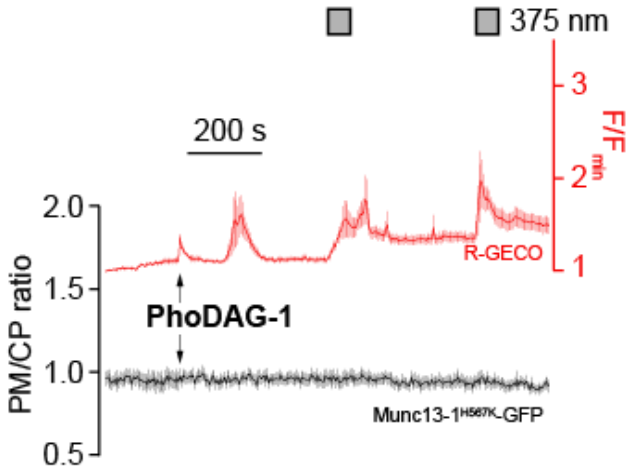

Supplementary Figure 14 | A C1 domain point mutant abolishes the sensitivity of Munc13-1 to PhoDAG-1. In HeLa cells, The DAG-insensitive Munc13-1^{H567K}-GFP mutant translocation reporter did not translocate on the application of **PhoDAG-1** (150 μM) or after photoactivation with λ = 375 nm light, even though an increase in $[Ca^{2+}]_i$ levels was observed (n = 13).

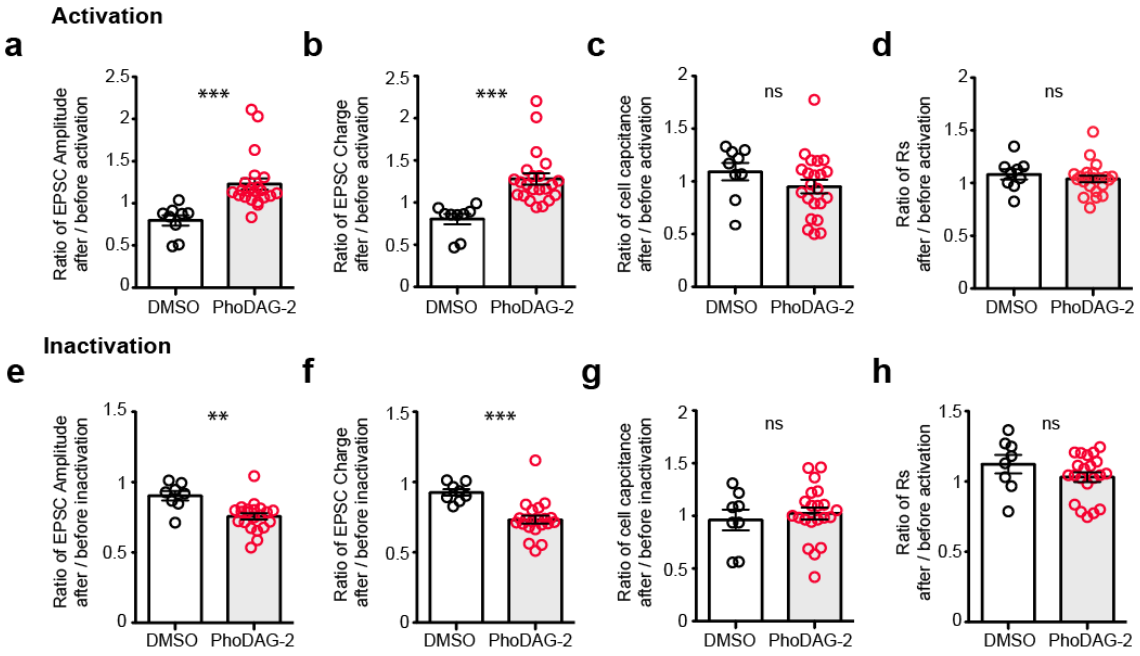

Supplementary Figure 15 | PhoDAG-2 application does not affect the pipette series resistance in patch-clamp experiments. PhoDAG-2 and **PhoDAG-3** are lipid compounds, and therefore might affect the series resistance of the patch pipette, which could lead to artifacts in the EPSC amplitude. Moreover, the compound integrates in the cell membrane where it might lead to changes in the cell size or membrane conductance. To exclude these effects, we performed a control experiment with **PhoDAG-2** and monitored series resistance and membrane capacitance, before and after illumination (n represents the number of illumination cycles; DMSO, black, for activation n = 9, for inactivation n = 8; **PhoDAG-2**, red, for activation n = 22, for inactivation n = 21). (**a**) The ratio of the change in the EPSC amplitude was calculated by dividing the average amplitude after photoactivation, by that before photoactivation. (**b**) The ratio of the change in EPSC charge was calculated by dividing the average charge after activation by that before activation. (**c**) The ratio of the change in the cell capacitance, a measure of the cell body size and conductance, was calculated by dividing the average capacitance after activation by that before activation. (**d**) The ratio of the change in series resistance was calculated by dividing the average capacitance after activation by that before activation. (**e**) The ratio of the change in EPSC amplitude after inactivation. (**f**) The ratio of the change in EPSC charge after inactivation (**g**) The ratio of the change in cell capacitance after inactivation. (**h**) The ratio of the change in series resistance after inactivation. Error bars were calculated as s.e.m.; ns = not significant P>0.05, **P<0.01, ***P<0.001.

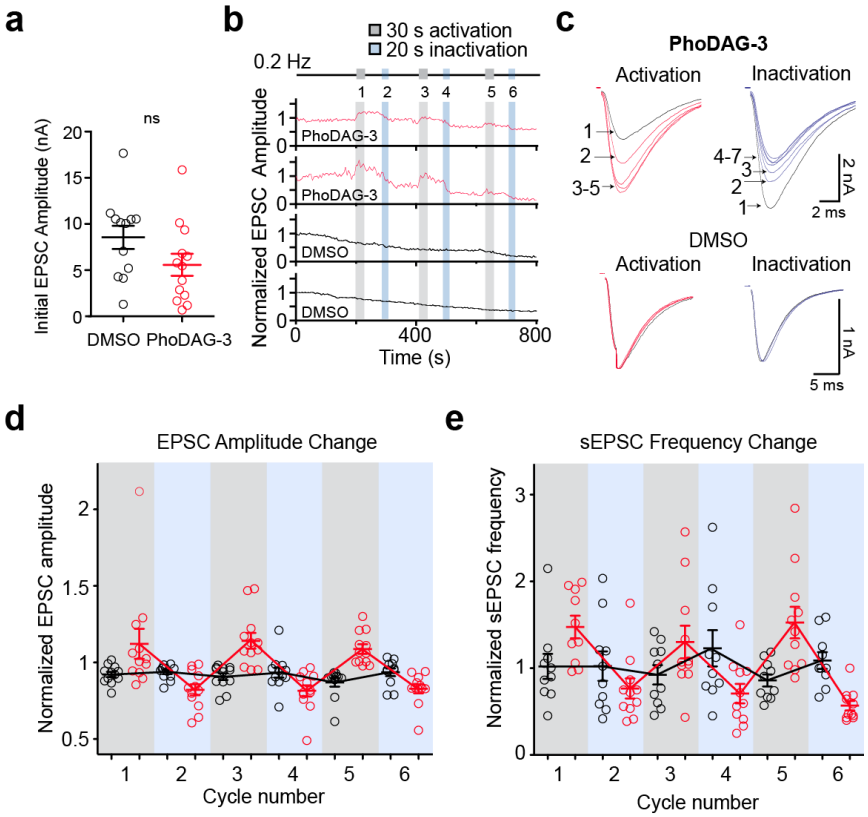

Supplementary Figure 16 | PhoDAG-3 modulates synaptic transmission in hippocamcal neurons. WT mouse hippocampal neurons were pre-incubated at 37 ºC in the extracellular recording solution containing 500 μM **PhoDAG-3** or DMSO. The neurons were then whole-cell voltage clamped at room temperature and stimulated at 0.2 Hz. The evoked EPSCs were monitored. (**a**) The initial EPSC amplitudes measured in control neurons (black, n = 12) or in neurons where *trans*-**PhoDAG-3** was applied (red, n = 13) are not significantly different. (**b**) The normalized EPSC amplitude is plotted for two neurons preincubated with **PhoDAG-3** (red) and for two control neurons (black). (**c**) Example traces of EPSCs during activation and inactivation for **PhoDAG-3**. (**d**) Activation and inactivation by **PhoDAG-3** could be repeated over several cycles, corresponding to an increase and decrease in the EPSC amplitude, respectively (red = **PhoDAG-3**, n = 13; black = vehicle, n = 12). (**e**) The sEPSC frequency could also be increased by photoactivation with UV-A light, and decreased by inactivation with blue light (red = **PhoDAG-3**, n=11; black = vehicle, n=10). Data from individual neurons are presented by open circles, summaries are presented as mean ± s.e.m. The Mann-Whitney test was used to determine statistical significance. ns = not significant P>0.05.

NMR SPECTRA

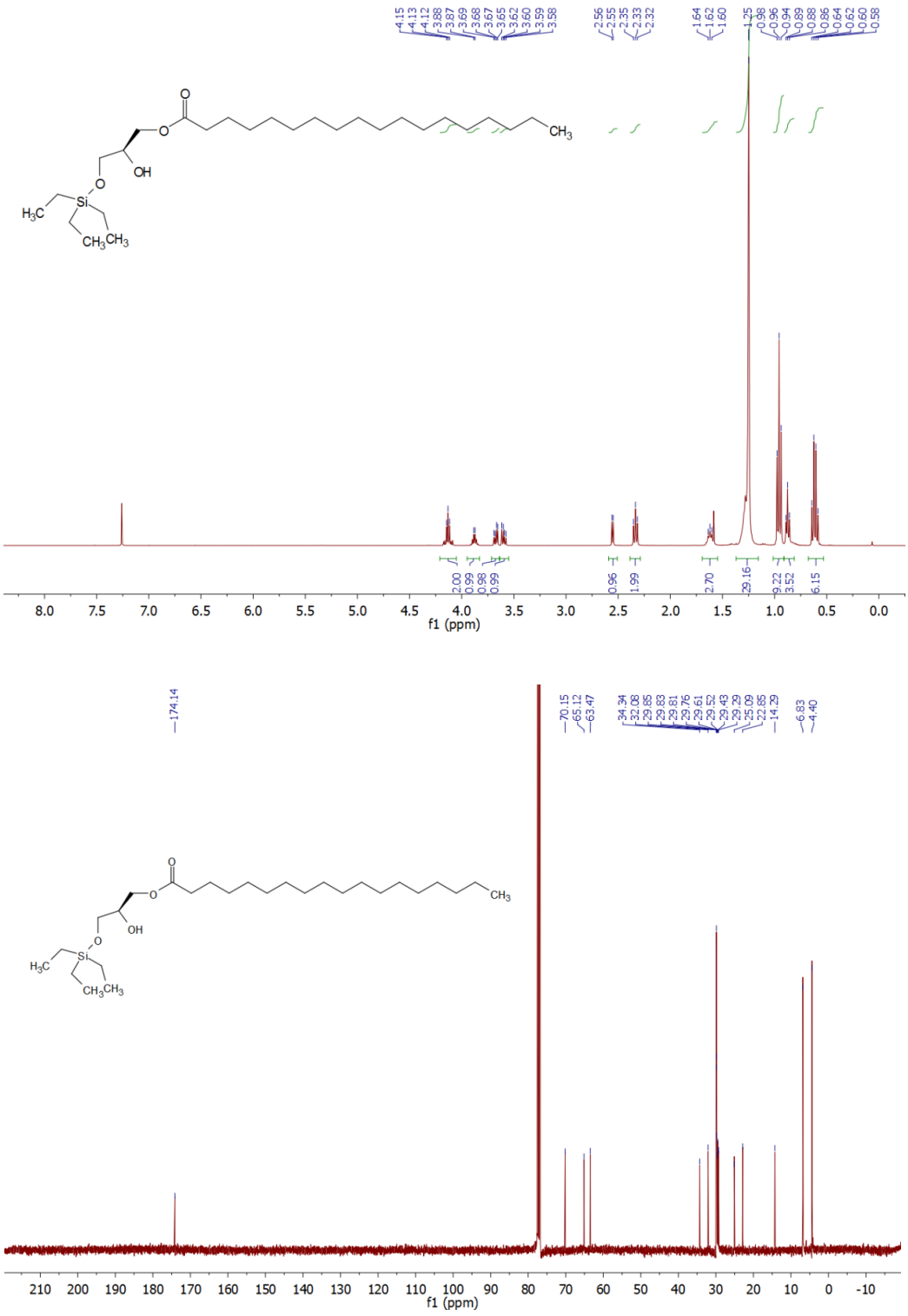

Supplementary Figure 17 | ^{1}H- and ^{13}C-NMR spectra of **1-*O*-stearoyl-3-*O*-triethylsilyl-*sn*-glycerol** (**3**).

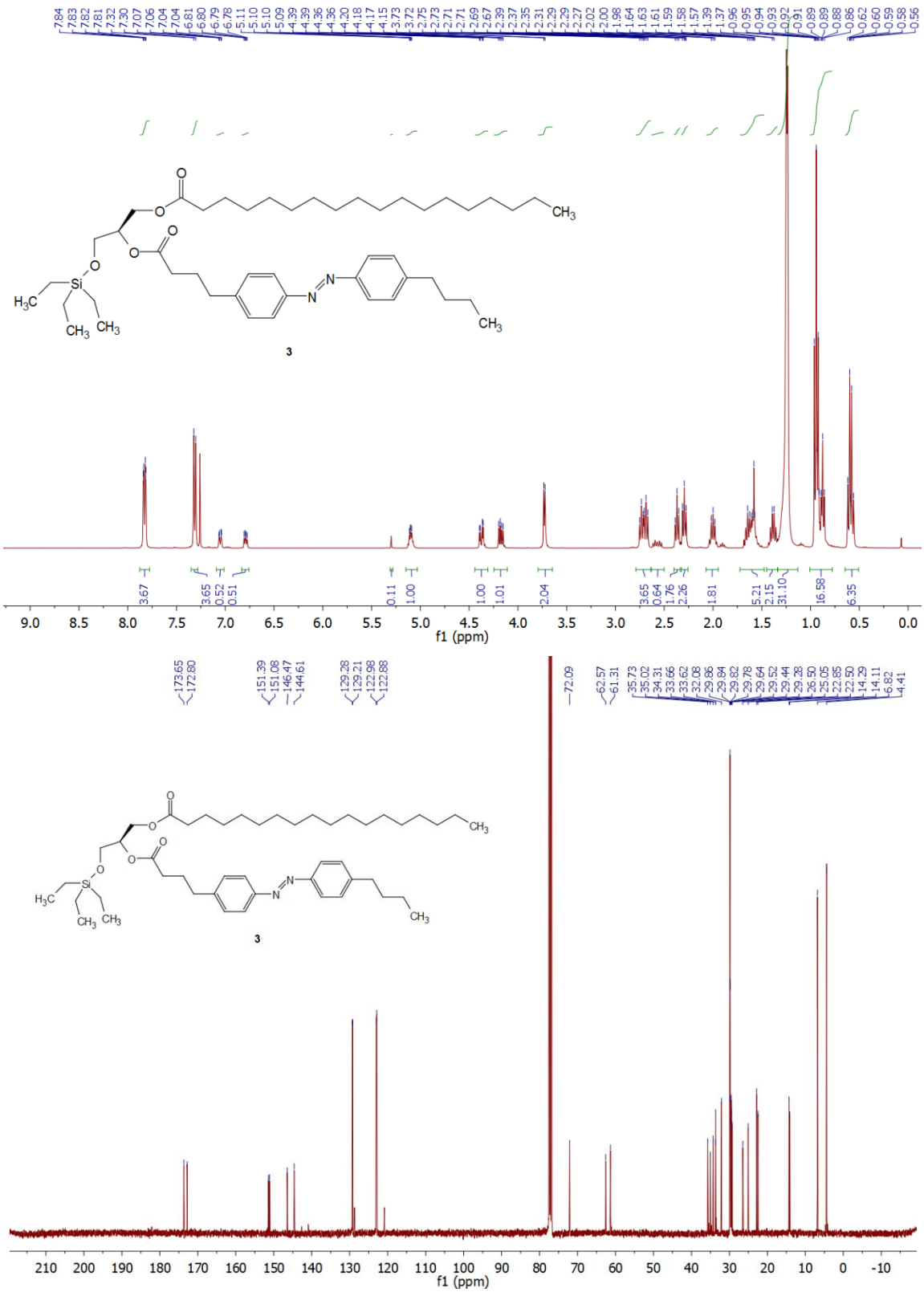

Supplementary Figure 18 | ^{1}H- and ^{13}C-NMR spectra of 2-*O*-(4-(4-((4-butylphenyl)diazenyl) phenyl)butanoyl)-1-*O*-stearoyl-3-*O*-triethylsilyl-*sn*-glycerol (**4**).

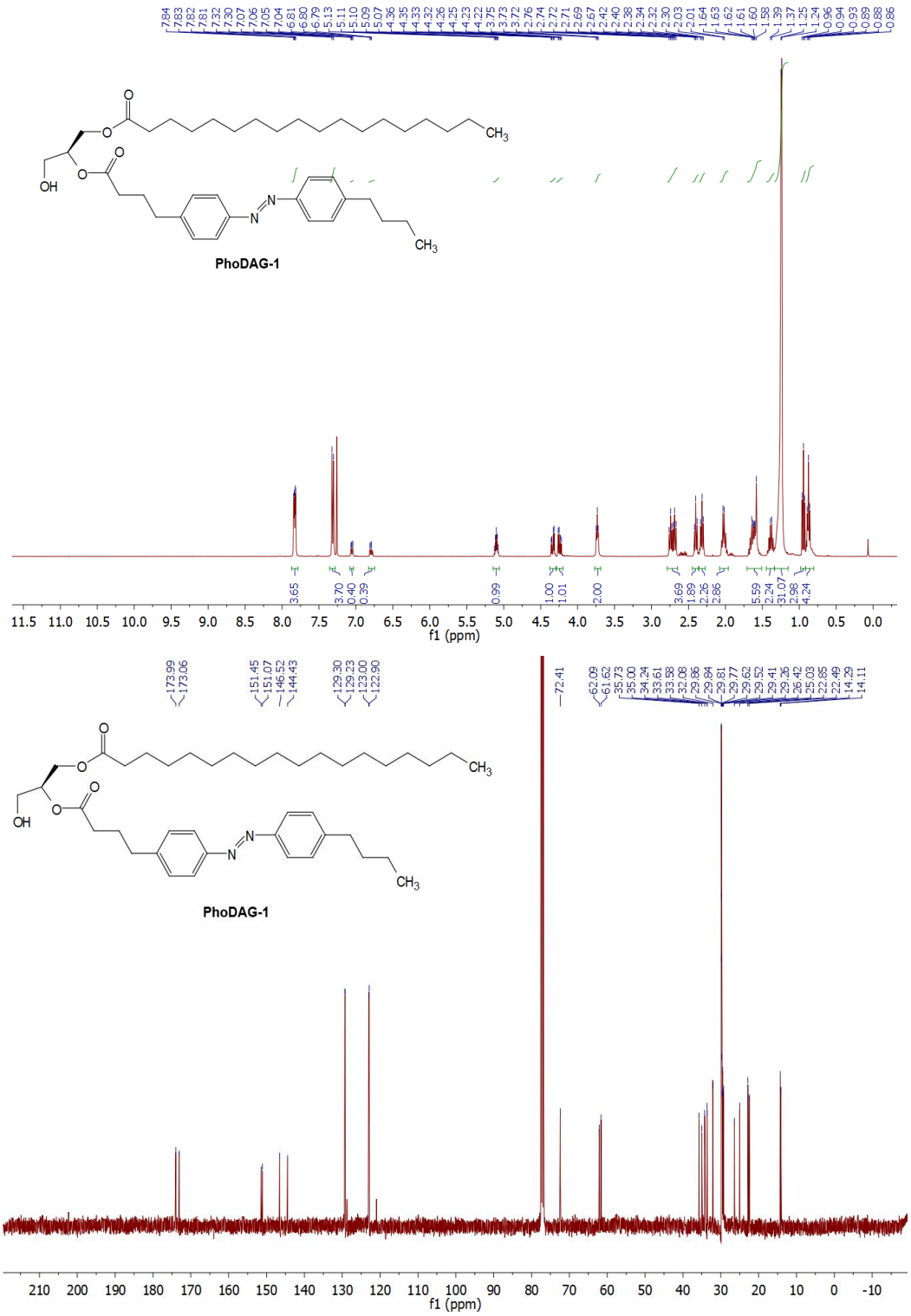

Supplementary Figure 19 | ^{1}H- and ^{13}C-NMR spectra of 2-*O*-(4-(4-((4-butylphenyl)diazenyl) phenyl)butanoyl)-1-*O*-stearoyl-*sn*-glycerol (**PhoDAG-1**).

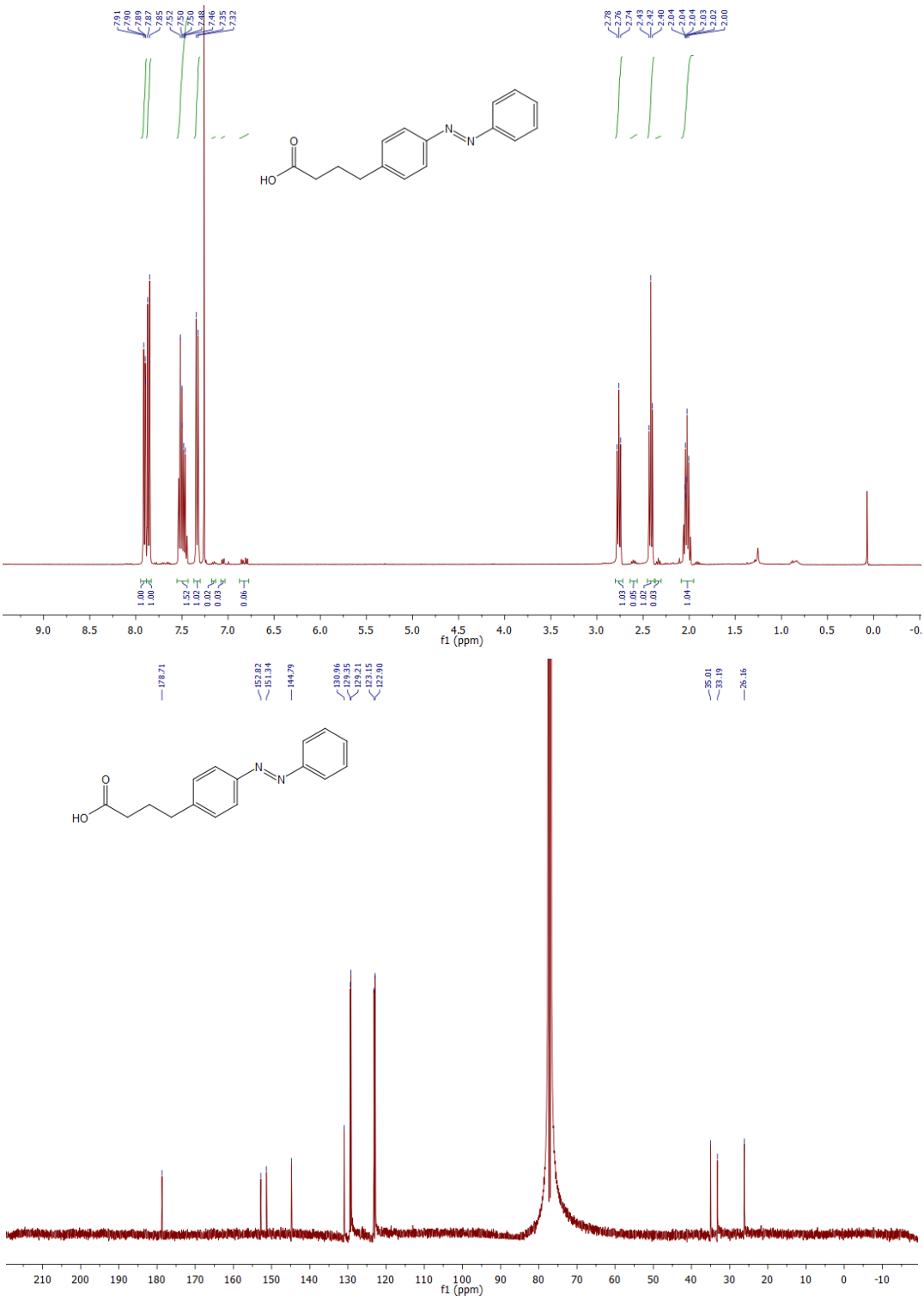

Supplementary Figure 20 | ^{1}H- and ^{13}C-NMR spectra of 4-(Phenyldiazenyl)phenyl butanoic acid (**FAAzo-9**).

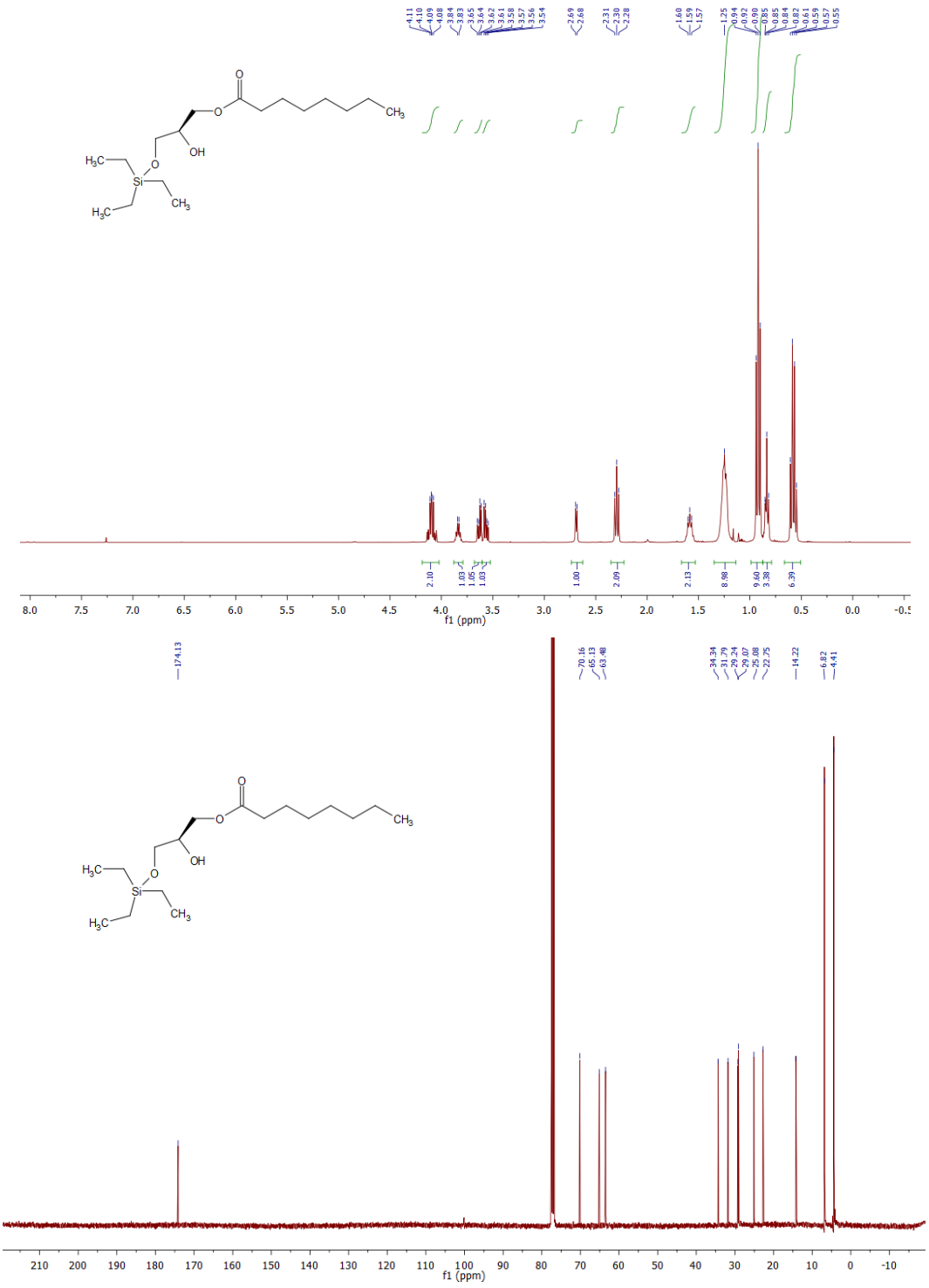

Supplementary Figure 21 | ^{1}H- and ^{13}C-NMR spectra of 1-*O*-octanoyl-3-*O*-triethylsilyl-*sn*-glycerol (**6**).

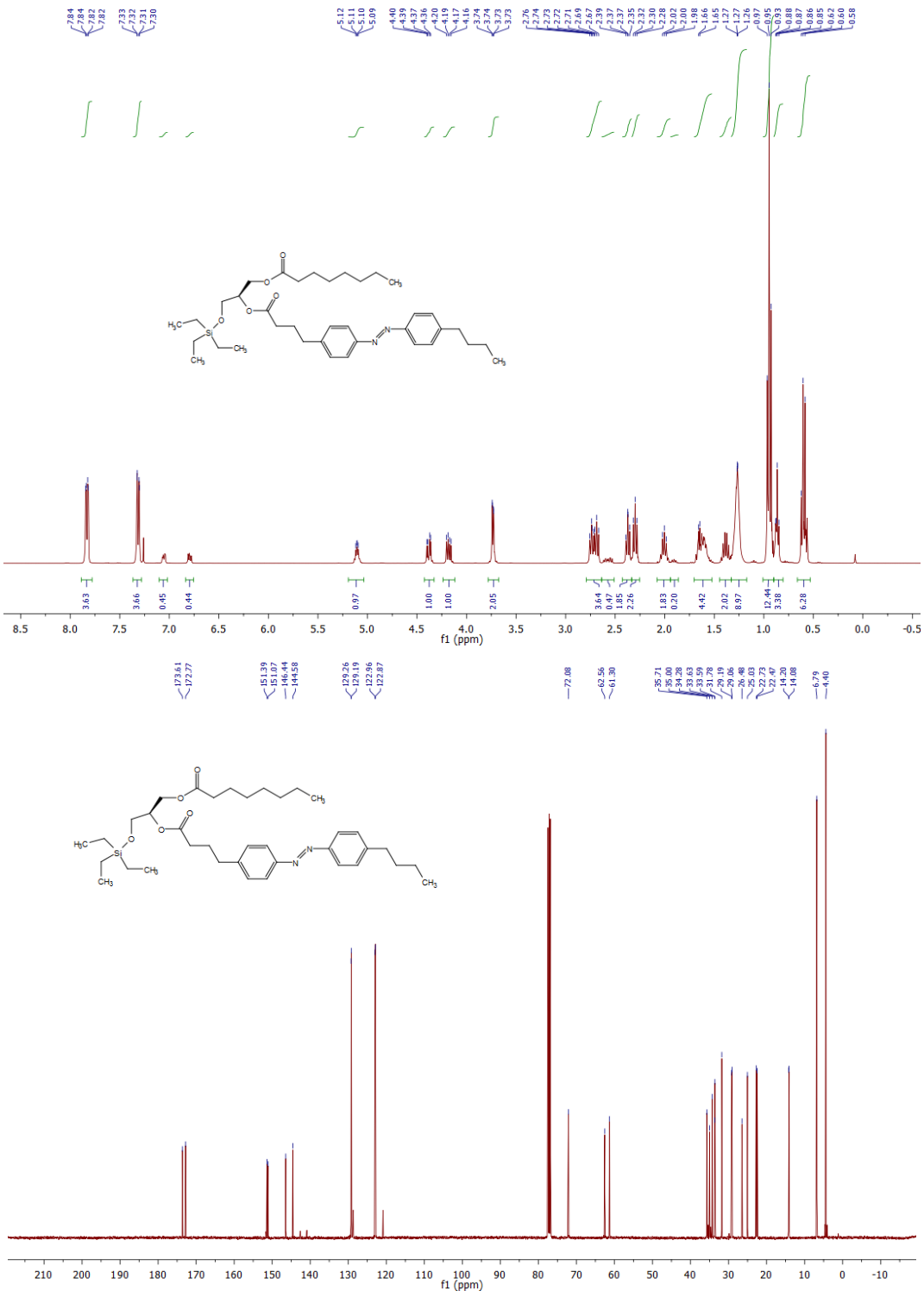

Supplementary Figure 22 | ^{1}H- and ^{13}C-NMR spectra of 2-*O*-(4-(4-((4-butylphenyl)diazenyl)phenyl) butanoyl)-1-*O*-octanoyl-3-*O*-triethylsilyl-*sn*-glycerol (**7**).

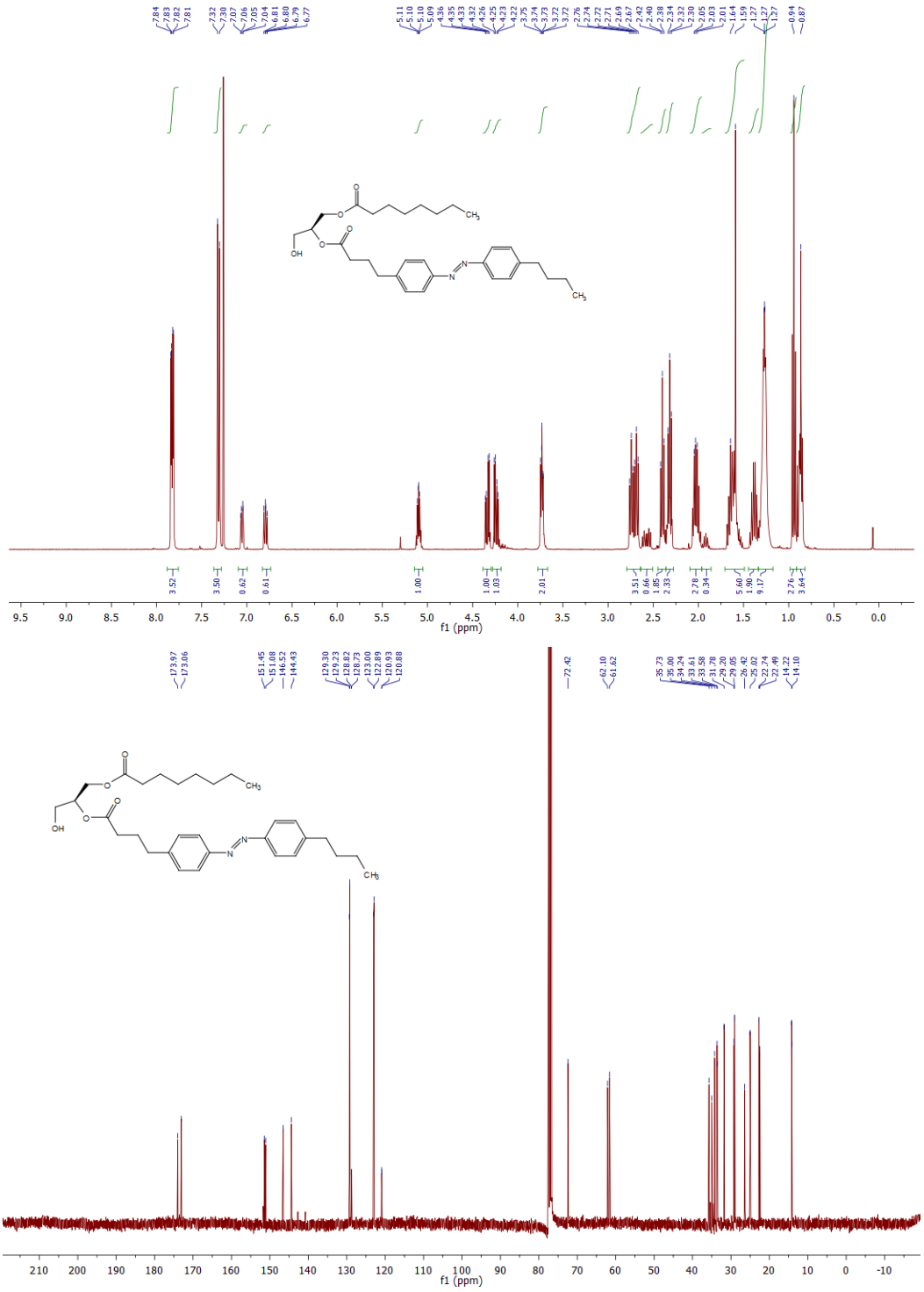

Supplementary Figure 23 | ^{1}H- and ^{13}C-NMR spectra of 2-*O*-(4-(4-((4-butylphenyl)diazenyl) phenyl)butanoyl)-1-*O*-octanoyl-*sn*-glycerol (**PhoDAG-2**).

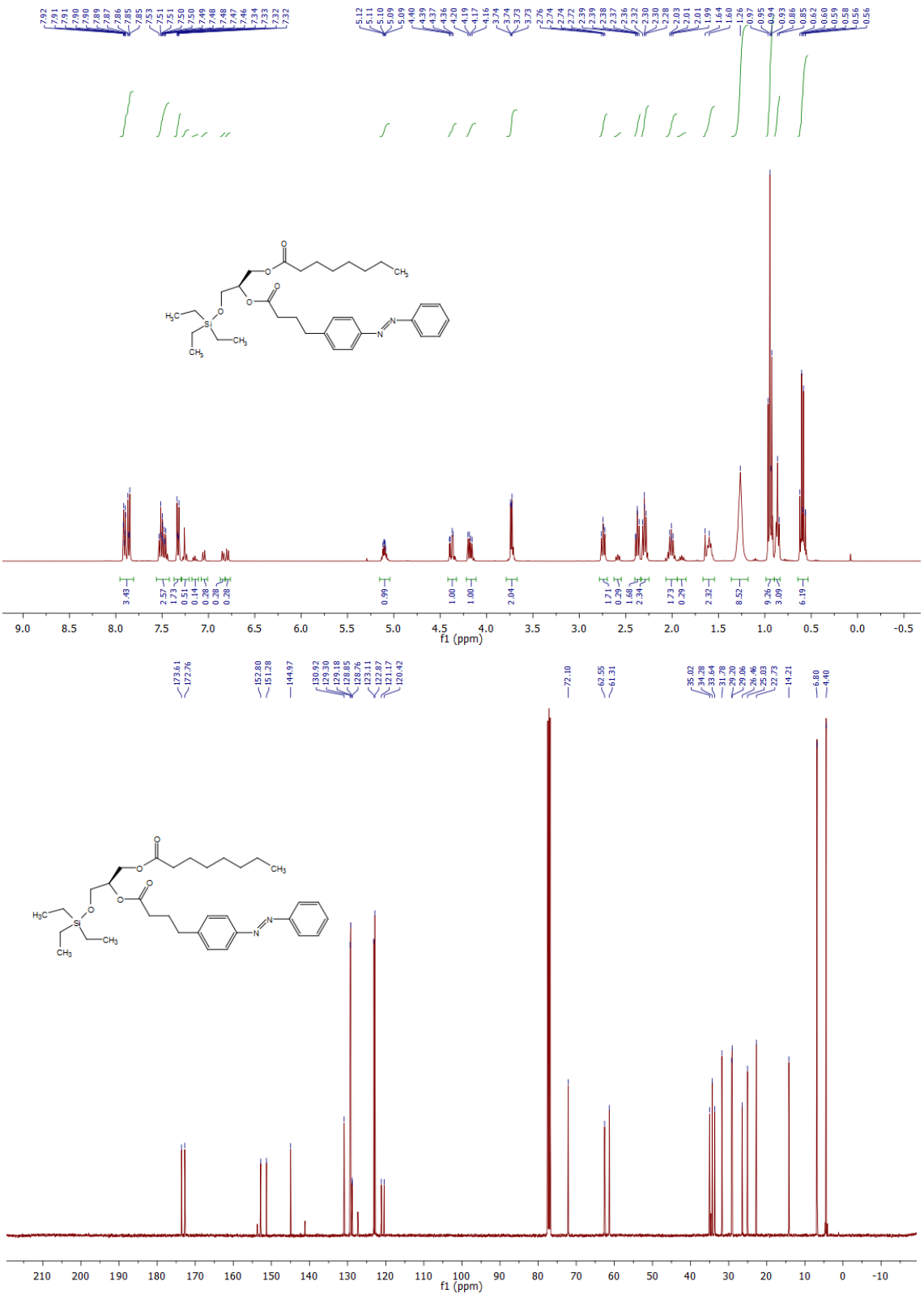

Supplementary Figure 24 | ^{1}H- and ^{13}C-NMR spectra of 2-*O*-(4-(4-(phenyldiazenyl)phenyl)butanoyl)-1-*O*-octanoyl-3-*O*-triethylsilyl-*sn*-glycerol (**8**).

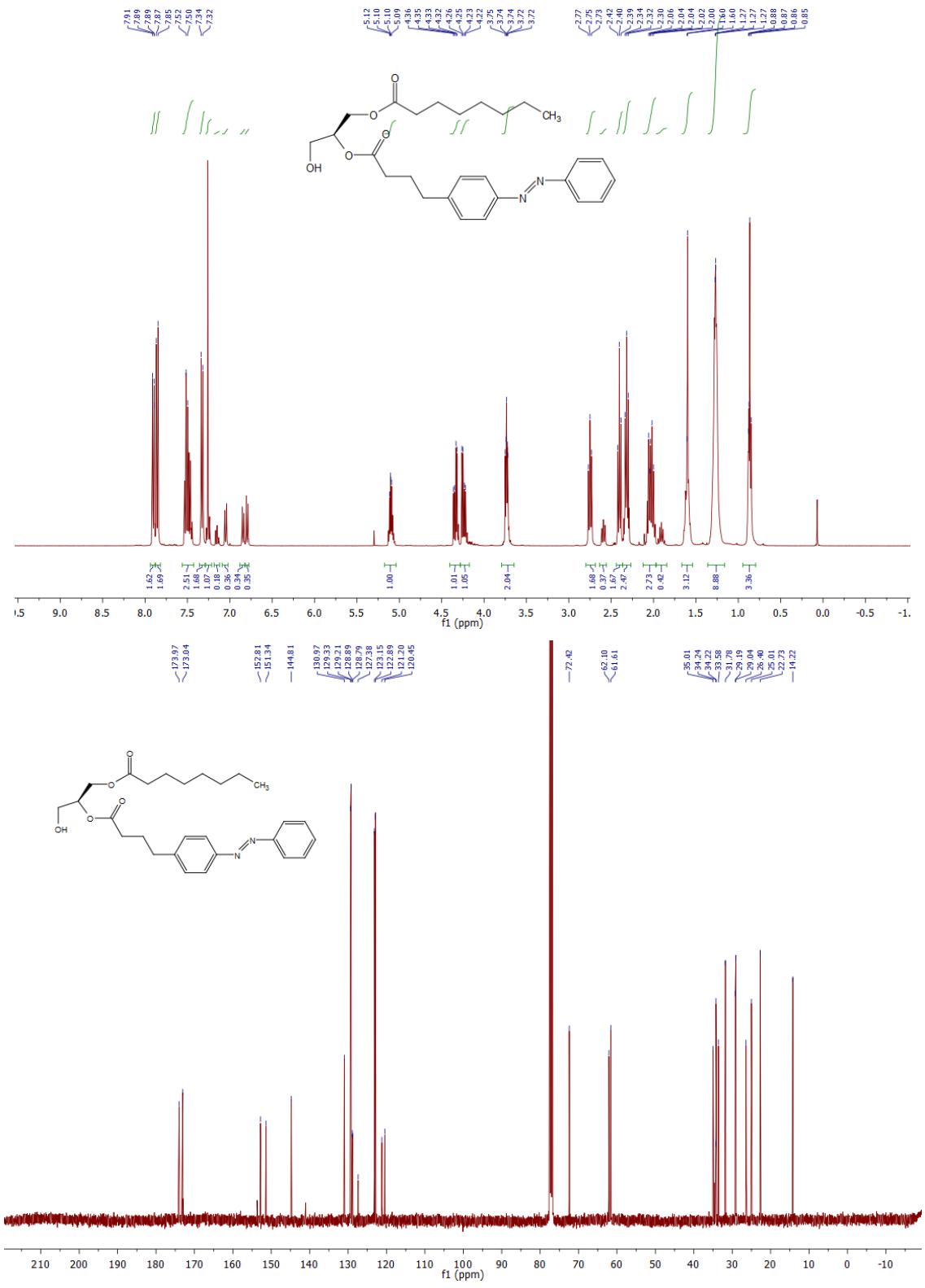

Supplementary Figure 25 | ^{1}H- and ^{13}C-NMR spectra of 2-*O*-(4-(4-(phenyldiazenyl) phenyl)butanoyl)-1-*O*-octanoyl-*sn*-glycerol (**PhoDAG-3**).

Supplementary Movie 1 | PhoDAG-1 enabled optical control of PKCδ-RFP translocation. A representative stack of fluorescence images showing PKCδ-RFP fluorescence in HeLa cells transiently expressing the reporter. The application of **PhoDAG-1** (red circle, 100 μM) did not affect the localization of PKCδ-RFP. On λ = 375 nm irradiation, PKCδ-RFP translocated to the plasma membrane. After the termination of irradiation, PKCδ-RFP diffused back to the cytoplasm. This effect could be repeated over multiple cycles. Each frame was acquired in 4 s intervals, and the video is played back at 6 fps.